Contact Resistance of 3D-Printed Interconnects to Thin-Film Metals for Advanced Packaging

Jacob Dawes, Alyssa Estenson, and Matthew L. Johnston
School of Electrical Engineering and Computer Science, Oregon State University, Corvallis, OR, USA
Email: dawesj@oregonstate.edu, estensoa@oregonstate.edu , matthew.johnston@oregonstate.edu

***Abstract*—High resolution 3D-printing of conductive inks has shown promise in enabling rapid prototyping for package scale interconnects and devices. If additive manufacturing becomes broadly adopted for package and chip-scale prototyping, it is critical to investigate contact resistance between printed materials and IC bond pad materials. In this work, contact resistance between direct-write printed silver interconnects and common IC contact materials (aluminum copper, gold) was measured across a range of ink thermal cure conditions. While contact resistance to gold and copper pads was largely dominated by sheet resistance and improved with increased cure time and temperature, contact resistance to aluminum pads was an order of magnitude larger, and increased with increasing cure time and temperature.**

I. Introduction

Additive manufacturing is poised to enable rapid development cycles in advanced packaging, particularly for fabrication of microwave and mm-wave structures [1], [2], development of flexible/stretchable packages [3], [4], and direct-write printing of integrated circuit (IC) interconnects [5]. The bulk material properties of the printed conductors, such resistivity and sheet resistance, are usually well characterized by conductive ink manufacturers. Investigations of contact resistance for printed interconnects has been more limited, however, such as thermosonic bonding of ICs to paper substrates [6] or low temperature soldering to printed PCBs [7]. There is a dearth of more generalized data in the literature on contact quality between printed metallic interconnects and conventional IC bond pad materials. For 3D-printed IC interconnects and fanout to prove viable as a rapid prototyping tool at the package level, it is critical to assess the contact resistance between printed interconnects and chip-level contacts.

In this work, we present an experimental study of the contact resistance between printed metallic interconnects and common CMOS IC bondpad materials toward 3D-printed IC interconnects in advanced packaging. A stacked cross method was used to compare the contact resistance between 3D-printed printed silver (Ag) traces and gold (Au), copper (Cu), or aluminum (Al) thin-film contacts and direct-write, for contact areas ranging from 5.14×10^3-3.45×10^4 μm^2, conducted over several cure times and temperatures. Printed interconnects were also compared against thermally evaporated thin-film interconnects in order to determine whether sheet resistance or interface contact resistance is dominant for each material.

II. 3D-Printed to Thin-Film Contact Structures

Several different structures are commonly used for measuring contact resistance. A transmission line method (TLM) has been used to measure contact resistance between printed metals and semiconductors, particularly for application in photovoltaics [8], [9]. Kelvin structures allow direct measurement of interface contact resistance over a wide range of contact resistances, although they require precise alignment of metal layers to achieve reliable measurements [10]. A stacked cross topology is easy to fabricate and is misalignment tolerant, although it can result in higher than expected estimates of contact resistance for samples with especially low contact resistance due to current crowding.

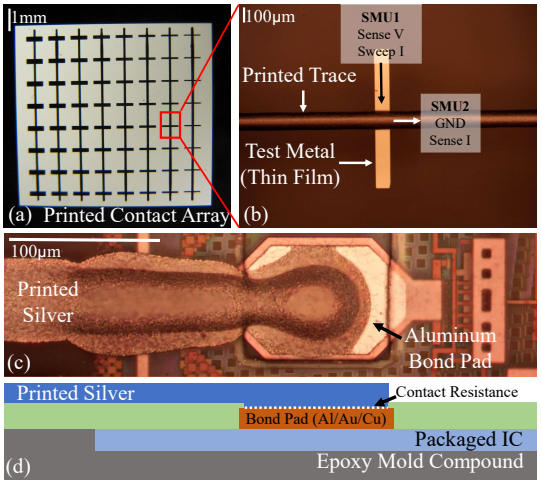

Fig. 1. (a) Two 8x8 contact arrays were fabricated for each test metal, along with thin film replicas. (b) Microscope image of sample contact..(c) Example of printed interconnect on a fan-out wafer-level package. (d) Cross section cartoon of example contact.

For this study, a stacked cross topology was used, as shown in Fig. 1. For each metal under investigation {Al, Au, Cu}, an 8×8 grid of contacts (8 test metal widths, each with 8 replicates) was fabricated. Fused silica wafers were spin coated with a layer of lift-off resist (LOR5B) followed by a layer of photoresist (S1813). After exposure and development defining the contact grid, a 200 nm layer of each metal was thermally evaporated to the substrate. Copper and gold were both deposited following an 20 nm chromium adhesion layer. Lift-off was performed using Remover PG, followed by cleaning.

Following test metal fabrication, traces were printed using silver ink (Novacentrix HPS-FG77) and a high-resolution 3D printer (nScrypt 3Dn) with a $50\,\mu m$ inner diameter ($75\,\mu m$ outer diameter) nozzle to form traces $\sim 100\mu m$ wide.

Control samples were prepared for each test metal using equivalently patterned gold-on-gold (20/200 nm Cr/Au) contact arrays. 200 nm thick, $100\,\mu m$ wide traces of each test

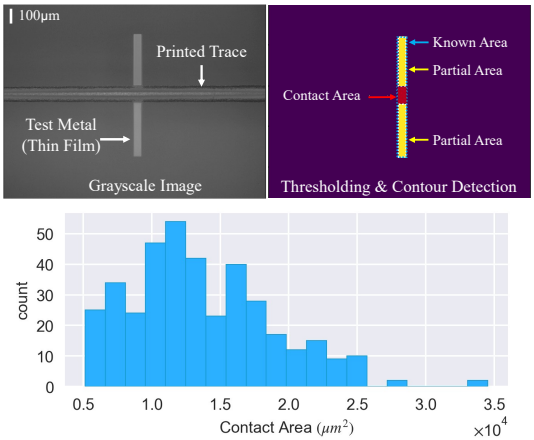

Fig. 2. Method for measuring contact area. Images are converted to grayscale, and thresholding is used to determine area of exposed metal. Those areas are subtracted from the known area of the test metal structure to determine contact area. Below is a histogram of the contact areas used in the study.

metal were then lithographically defined on top using a similar lift-off process. Any metals requiring adhesion layers were evaporated with a thinner layer of chromium (1/200 nm Cr/Au and Cr/Cu) to decrease the impact of its resistivity observed at the contact interface. While the control samples do not account for the sheet resistance of the printed traces, they provide a standard baseline for comparison of printed samples.

III. Measuring Contact Resistance

To measure the contact resistance, a four-wire probe setup was used connected to a Keithley Semiconductor Parameter Analyzer. Each 8×8 grid of test contacts was imaged, and contact areas were extracted as below.

A. Measuring Contact Area

To account for variable contact area, both resulting from the design of the contact arrays and print variability, all contact areas were estimated independently using the method shown in Fig. 2. Each test contact was imaged under a microscope after printing and curing, and openCV was used to measure the area of test metal covered by the printed trace. Since the thin-film metal appears brighter than the printed trace, thresholding can be used to remove all parts of the image except those containing the metal. Contour detection was then used to detect the edges of all metal objects, which were sorted by size. Finally, the area of metal objects in the image was subtracted from the area of each test metal, determining the contact area.

B. Four-Wire Resistance Measurements

To measure resistance of each contact, one source measure unit (SMU) was connected to each test metal pad and another connected to the printed trace (or control trace) using pairs of tungsten needle probes. Both sets of probes are landed as close as possible to the contact under test to minimize added series resistance. For all measurements, one SMU was configured to force GND (0V) while sensing current, and another was set to force a current (swept $100 - 500\,\mu A$) while sensing voltage.

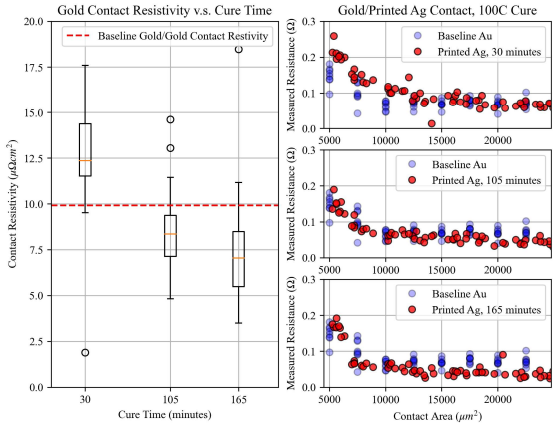

Fig. 3. Resistance and contact resistivity measurements between printed silver traces and gold pads across contact area and cure time.

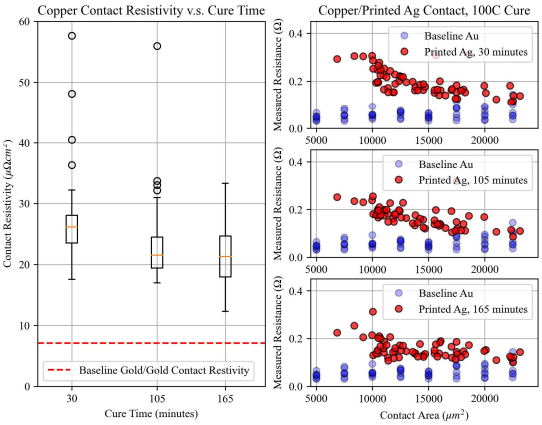

Fig. 4. Resistance and contact resistivity measurements between printed silver traces and copper pads across contact area and cure time.

Using this four-probe setup, probe contact resistance and cable resistance are effectively eliminated from the measurement.

IV. Print-to-Thin-Film Contact Resistance

Printed Ag inks typically undergo a low-temperature curing process to improve conductivity. While longer cure times and hotter temperatures typically result in lower sheet resistance,

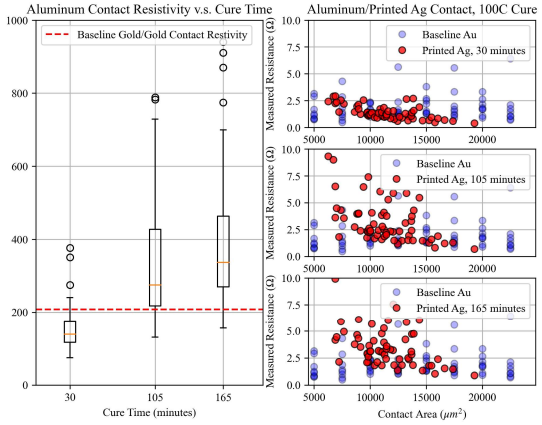

Fig. 5. Resistance and contact resistivity measurements between printed silver traces and aluminum pads across contact area and cure time.

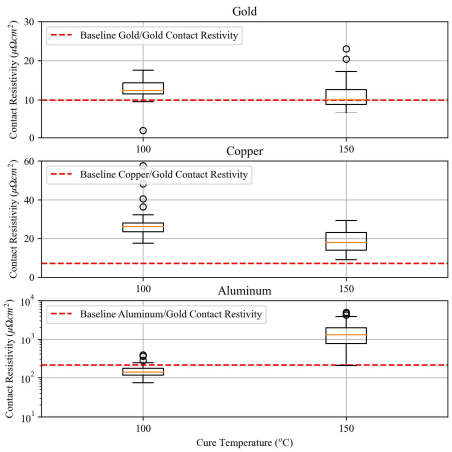

Fig. 6. Contact resistivity between all three test metals and printed silver traces, compared over two temperatures. Log scale was used on the aluminum data due to large difference in resistivity magnitude.

the effect on contact resistivity is unknown. As such, for each test metal, two samples were prepared and cured at 100 °C and 150 °C, respectively. The samples cured at 100 °C were cured for a total of 165 minutes, measured at 30 minutes, 105 minutes, and 165 minutes. The samples cured at 150°C were measured at 30 minutes.

Measured results for gold and copper contacts are shown in Fig. 3 and Fig. 4 respectively. The measured resistance was comparable with both the control sample and the known sheet resistance of the metal stack. To calculate contact resitivity, measured resistance was multiplied by extracted contact area. For both materials, as cure time increases, the resistance decreases (with diminishing return), reflecting the expected change in sheet resistance of printed traces. For aluminum contacts, shown in Fig. 5, the measured resistances were much larger. For the 100 °C samples, total resistance was much larger due to higher sheet resistance, and contact resistance becomes increasingly significant as bake time increases.

The effects of cure temperature, shown in Fig. 6, are similar to those of cure time. For the copper and gold samples, cure temperature results in a lower resistance contact, likely as a result of decreased sheet resistance. For the aluminum, increased cure temperature results in an order of magnitude increase in contact resistivity. While the data in this work do not separate interface contact resistance from the sheet resistance at the contact, the contribution of interface contact resistance may be practically neglected if it is significantly lower than the sheet resistance of the film.

Overall, the contact resistance between 3D-printed silver traces and thin-film aluminum is an order of magnitude worse than for gold or copper thin-films, likely due to the native oxide. This is of particular note given that many commercial CMOS processes provide aluminum bondpads; while the native oxide is broken during ultrasonic wirebonding, this is not the case during printing, and alternate approaches may be needed to print IC interconnects with low contact resistance.

V. Conclusion

In this work, we present measured results from a study of contact resistance between 3D-printed conductive ink and common IC bond pad materials. For copper and gold contacts, printed Ag traces appear to have comparable contact resistance to evaporated thin-film contacts, and measured resistance is dominated by sheet resistance. For these materials, longer and hotter cure times increase the conductivity of the printed materials, thus improving the overall contact quality. In the case of aluminum contacts, the measured resistance is dominated by resistance at the contact interface, likely due to the native oxide layer, leading to markedly worse contact quality. If aluminum contacts are used, which are common in IC bond pads, shorter, cooler curing may be necessary to decrease contact resistance at the cost of added sheet resistance, and additional processing steps may be required to disrupt the native oxide and protect the aluminum surface prior to or during 3D-printing.

References

[1] E. A. Rojas-Nastrucci, R. Ramirez, D. Hawatmeh, D. Lan, J. Wang, and T. Weller, "Laser enhanced direct print additive manufacturing for mm-wave components and packaging," in *2017 International Conference on Electromagnetics in Advanced Applications (ICEAA)*. IEEE, 2017, pp. 1531–1534.

[2] B. K. Tehrani, R. A. Bahr, and M. M. Tentzeris, "Inkjet and 3D printing technology for fundamental millimeter-wave wireless packaging," *Journal of Microelectronics and Electronic Packaging*, vol. 15, no. 3, pp. 101–106, 2018.

[3] T.-H. Lin, S. N. Daskalakis, A. Georgiadis, and M. M. Tentzeris, "Achieving fully autonomous system-on-package designs: An embedded-on-package 5g energy harvester within 3d printed multilayer flexible packaging structures," in *2019 IEEE MTT-S International Microwave Symposium (IMS)*. IEEE, 2019, pp. 1375–1378.

[4] S. Ma, A. S. Dahiya, and R. Dahiya, "Direct write 3d-printed interconnects for heterogenous integration of ultra thin chips," in *2022 IEEE International Conference on Flexible and Printable Sensors and Systems (FLEPS)*. IEEE, 2022, pp. 1–4.

[5] J. Dawes and M. L. Johnston, "Direct-write 3D printing of interconnects for fan-out wafer-level packaging," in *2022 IEEE International Conference on Flexible and Printable Sensors and Systems (FLEPS)*. IEEE, 2022, pp. 1–4.

[6] A. Roshanghias, A. D. Rodrigues, and D. Holzmann, "Thermosonic fine-pitch flipchip bonding of silicon chips on screen printed paper and pet substrates," *Microelectronic Engineering*, vol. 228, p. 111330, 2020.

[7] J. Jäger, S. Buschkamp, K. Werum, K. Gläser, T. Grözinger, W. Eberhardt, and A. Zimmermann, "Contacting inkjet-printed silver structures and smd by ica and solder," *IEEE Transactions on Components, Packaging and Manufacturing Technology*, vol. 12, no. 7, pp. 1232–1240, 2022.

[8] D. R. Rowell, J. D. Wood, C. L. Stender, R. Chan, A. Wibowo, M. Osowski, and N. Pan, "Screen printed silver contacts on iii-v bulk pseudomorphic and lifted off thin film foils for high volume low cost solar cell manufacturing," in *2020 47th IEEE Photovoltaic Specialists Conference (PVSC)*. IEEE, 2020, pp. 1531–1533.

[9] J. D. Wood, C. L. Stender, C. T. Youtsey, D. Rowell, A. Wibowo, M. Osowski, and N. Pan, "Screen printed contacts to iii-v epilayers for low cost photovoltaics," in *2018 IEEE 7th World Conference on Photovoltaic Energy Conversion (WCPEC)(A Joint Conference of 45th IEEE PVSC, 28th PVSEC & 34th EU PVSEC)*. IEEE, 2018, pp. 3853–3856.

[10] H. Lin, S. Smith, J. Stevenson, A. Gundlach, C. Dunare, and A. Walton, "An evaluation of test structures for measuring the contact resistance of 3-d bonded interconnects," in *2008 IEEE International Conference on Microelectronic Test Structures*. IEEE, 2008, pp. 123–127.